Arun Kumar Pujari*, B. V. S. S. S Prasad and Nekkanti Sitaram

Conjugate Heat Transfer Analysis on the Interior Surface of Nozzle Guide Vane with Combined Impingement and Film Cooling

Abstract: The effect of conjugate heat transfer is investigated on a first stage nozzle guide vane (NGV) of a high pressure gas turbine which has both impingement and film cooling holes. The study is carried out computationally by considering a linear cascade domain, having two passages formed between the vanes, with a chord length of 228 mm and spacing of 200 mm. The effect of (i) coolant and mainstream Reynolds numbers, (ii) thermal conductivity (iii) temperature difference between the mainstream and coolant at the internal surface of the nozzle guide vane are investigated under conjugate thermal condition. The results show that, with increasing coolant Reynolds number the lower conducting material shows larger percentage decrease in surface temperature as compared to the higher conducting material. However, the internal surface temperature is nearly independent of mainstream Reynolds number variation but shows significant variation for higher conducting material. Further, the temperature gradient within the solid thickness of NGV is higher for the lower conductivity material.

Introduction

The gas turbine engines are used in a wide range of applications such as aircraft propulsion, industrial power generation, and ship propulsion. The thermodynamic

*Corresponding author: Arun Kumar Pujari,** Thermal Turbomachines Laboratory, Department of Mechanical Engineering, Indian Institute of Technology Madras, Chennai 600036, India,
E-mail: akp327@gmail.com
B. V. S. S. S Prasad: E-mail: Prasad@iitm.ac.in, **Nekkanti Sitaram:**
E-mail: nsitaram@iitm.ac.in, Thermal Turbomachines Laboratory, Department of Mechanical Engineering, Indian Institute of Technology Madras, Chennai 600036, India

processes in a gas turbine are idealized by the Brayton cycle which comprises of compression followed by combustion and finally by the expansion of hot gases in the turbine. In order to achieve higher thermal efficiency and increase engine thrust, the increase in turbine inlet temperature is one of the key factors. While extracting the thermal energy from the hot gases the first stage high-pressure nozzle guide vanes (NGV) are exposed to hot gases of very high temperature. The increase in turbine inlet temperature will lead to higher thermo-mechanical stresses in the NGV. In order to reduce the thermal stress, it is essential to use enhanced cooling techniques and proper materials for the NGV. An efficient cooling system can be designed by the study of conjugate heat transfer, which couples the convective modes of heat transfers on the external and internal surfaces with that of conduction within the vane.

In an attempt to apply the surface temperature data of laboratory tested airfoils to the actual engine airfoils, the Biot number (h.t/k) of both should be matched. Bogard and co-workers [1–4] used the matched Biot number method to know overall effectiveness given by the expression

$$\text{Overall effectiveness,} \quad \phi = \frac{1}{\left(1 + \text{Bi} + \frac{h_e}{h_i}\right)} \tag{1}$$

for a cooled NGV.

They pointed out that, as the laboratory experiment is run at temperatures and pressures significantly below the engine conditions, the values of dimensional temperature and heat transfer coefficient are lower. Therefore, in order to match the normalized surface temperature values obtained at laboratory conditions with those at actual conditions, it is essential to use lower conductivity material with a range from 0.05 W/m.K to 1.2 W/m.K. This makes the Biot number to vary from 0.4 to 1.6 under the laboratory conditions. Ravelli et al. [5] investigated the influence of impingement cooling, on the overall cooling effectiveness of a turbine leading edge provided with three rows of film holes. They showed that the overall effectiveness is improved by the impingement cooling. This effect on overall effectiveness was due to conjugate effect. Nathan et al.

[6] also reported the adiabatic and overall effectiveness on the leading edge of a turbine vane and identified the hot spots on the vane leading edge using the overall effectiveness distribution. Montomoli et al. [7] considered the impingement on a circular cylinder made of polycarbonate and stainless steel, in order to highlight the impact of conduction on coolant effectiveness. They found lower thermal gradients and uniform effectiveness distribution for higher conducting material and hence recommended the same for reducing the thermal stresses in the cylinder. Panda and Prasad [8] studied the effect of solid thermal conductivity on conjugate heat transfer from a flat plate with combined impingement and film cooling. Williams et al. [9] conducted experiments on the suction side of a vane, by using two materials (k = 0.048 W/m.K and k = 1.1 W/m.K) and reported that the internal impingement cooling influences the overall effectiveness significantly.

From the above conjugate heat transfer studies on the flat plate and the airfoil surfaces, it is clear that the overall effectiveness is influenced by internal cooling. However, none of the researchers addressed the effect of thermal conductivity under conjugate conditions, and when the external and internal Reynolds numbers are varied.

In view of these observations, present computational work is taken up to obtain the spanwise averaged internal surface temperature and Nusselt number distributions at different coolant and mainstream Reynolds numbers. Variations of temperature gradient within the vane are also presented. All the computations are carried out at laboratory conditions, so as to validate the methodology, with the available experimental data.

Matched Biot number method

In a method similar to [4], the internal surface heat flux values can be expressed as

$$q'' = h_i(T_i - T_c) = \frac{(T_m - T_c)}{\left(\frac{1}{h_i} + \frac{t}{k} + \frac{1}{h_e}\right)} \qquad (2)$$

where T_i is the internal surface temperature and T_c is the coolant temperature.

The dimensionless temperature of the interior surface is given by

$$\theta = \frac{(T_i - T_c)}{(T_m - T_c)} = \frac{1}{\left(1 + \frac{t h_i}{k} + \frac{h_i}{h_e}\right)} = \frac{1}{\left(1 + Bi + \frac{h_i}{h_e}\right)} \qquad (3)$$

In the above expression the Biot number values are based on internal heat transfer coefficient. As the value of h_i/h_e is of the order unity, the value of thermal conductivity range needs to be from 0.05 W/m.K to 1.2 W/m.K and the corresponding Biot number from 0.4 to 1.6. These values ensure that the non-dimensional internal surface temperatures obtained from laboratory experiments are valid for engine conditions.

Physical model

In order to carry out the conjugate heat transfer analysis, a two-dimensional cascade with a space chord ratio of 0.88 is considered as shown in Figure 1(a). The details of the cascade domain are presented in Table 1. The domain
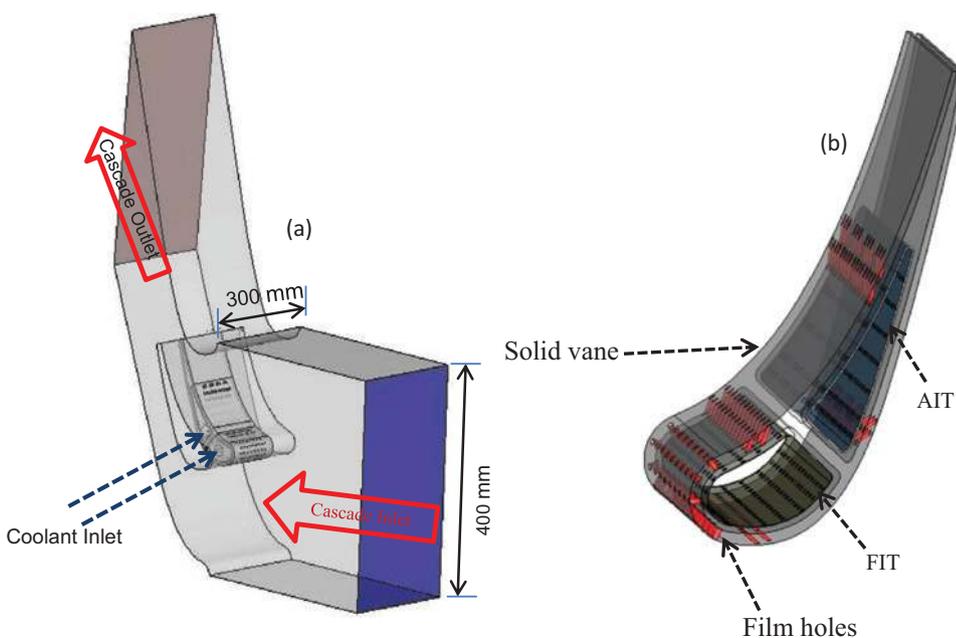

Figure 1: (a) Cascade flow domain (b) Vane with film and impingement holes.

Table 1: Details of cascade computational domain.

Span	800 mm
Axial chord	133.7 mm
Chord	228 mm
Stagger angle	54°
Aspect ratio	3.5
Space-chord ratio	0.88

of study contains two flow paths: one is the mainstream, and the other is coolant. The mainstream flow path is through the external cascade vane surfaces, typical of a gas turbine NGV. The domain is extended to 1.5 chord length both upstream and downstream of the vanes for the purpose of computations. The NGV has a combined impingement and film cooling configuration as shown in Figure 1(b). The total surface of the NGV is divided into four regions namely: the leading edge region (LER), fillet region (FR), midspan region (MR) and trailing edge region (TER) as shown in Figure 2(a). The non-dimensional surface lengths: NDL = zero corresponds to stagnation point at the leading edge, +1 corresponds to pressure surface and −1 corresponds to suction surface. The NGV is cooled internally by two jet impingement chambers. The front impingement chamber (FIT) is used to cool the leading region of the vane, whereas the mid-chord region of the vane is cooled by the aft impingement tube (AIT). The coolant impinges from both the suction side and pressure side holes (PSIH1 to PSIH 11 and SSIH 1 to SSIH 15) on the vane interior surface (Figure 2(b)). The coolant comes out through the film cooling holes (SS1 to SS6, SH, PS1 to PS6) at different regions as shown in Figure 2(c) and mixes with the mainstream.

Computational methodology

To carry out the conjugate heat transfer study, the cascade domain is split into three different zones, out of which two are main-stream and coolant fluid zones and one is vane solid zone. Formulation of three-dimensional conjugate heat transfer problem is made with the following assumptions: (i) the fluid is incompressible (ii) the fluid properties are constant, (iii) radiation and natural convection are neglected, (iv) viscous heating is absent and (v) the flow is steady.

The governing equations used for simulation are the Reynolds averaged continuity, momentum and the energy equations along with the equations for modelling the turbulence quantities. Boundary conditions used for the present study are: no slip at the walls, cascade inlet as velocity inlet, coolant inlet as mass flow inlet, cascade outlet boundary condition as pressure outlet ($P = P_{amb}$). All thermal conditions at vane surface as conjugate, $T_{solid} = T_{fluid}$ and $k_s \ (\partial T_s/\partial y) = k_f \ (\partial T_f/\partial y)$. Periodic boundary condition is given at the top and bottom wall of the domain so as to generate an infinite cascade model.

Mesh is generated in both the fluid and solid zones by grid generating tool available in Ansys ICEM CFD code as shown in Figure 3(a). Both tetrahedral and quadrilateral elements are used to mesh the cascade domain. In order to bring down the y+ value to be less than unity, very refined mesh is generated close to the vane surface by providing three-dimensional boundary layer type prismatic meshes as shown in Figure 3(b). The grid sensitivity study is carried out by
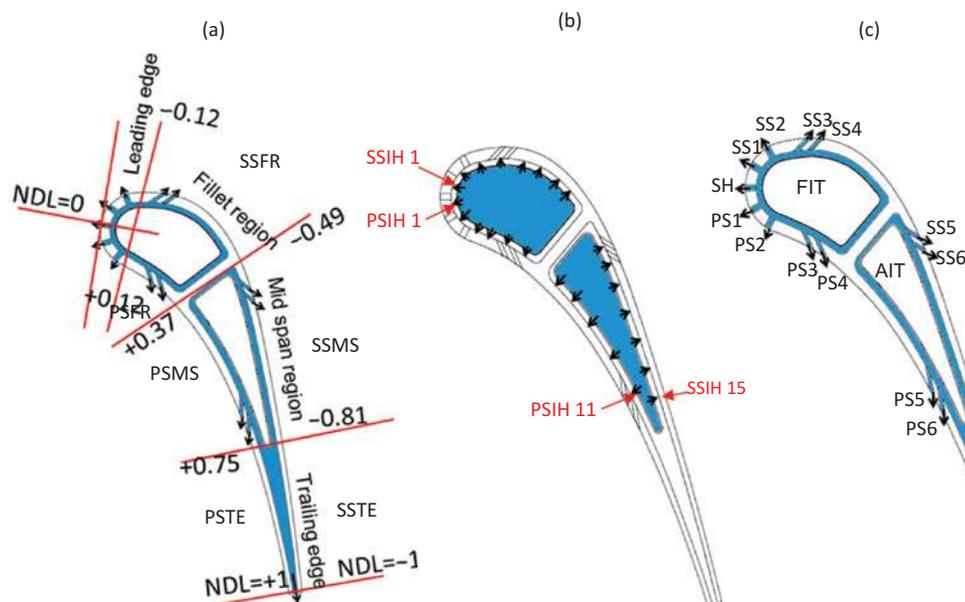

Figure 2: (a) Different regions of vane surface (b) Impingement locations (c) Film coolant flow locations.
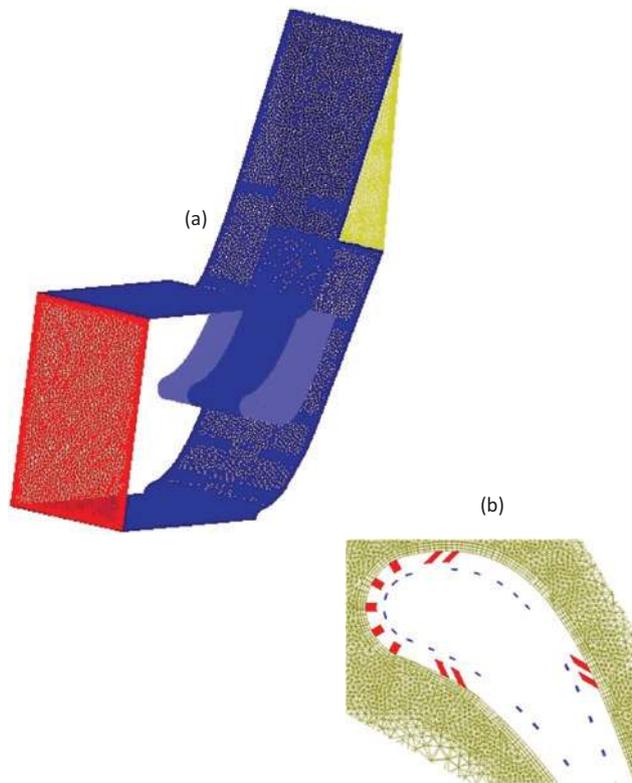
Figure 3: Details of the cascade flow domain and meshing (a) Flow domain meshing (b) Boundary layer mesh over the vane surface.

"grid convergence index" (GCI) method [10], to ensure consistency in the computational result. The GCI study is conducted with three meshes: coarse, medium and fine. The coarse mesh has approximately 8.8 million cells, and the wall y + is close to 2.1. The medium and fine meshes had cells close to 11.7 million and 13.8 million respectively, and their wall y + values were improved to 0.8 and 0.5 respectively by further refining the near wall zones. The medium mesh is found to be optimum and adopted for the present computational model.

Governing equations are solved using a finite volume based FLUENT 14 solver from the ANSYS 14 package. The κ (turbulent kinetic energy)-ω (specific dissipation) SST model is adopted for turbulence modeling, and SIMPLE algorithm is used for pressure-velocity coupling. The second order upwind scheme is used for momentum, energy, κ and ω. The solution is considered to be converged when the maximum residual value is in the order of 10^{-5} for continuity, and 10^{-6} for the momentum, turbulence quantities and the energy equation. Further, the area weighted average temperature of the target surface is continuously monitored so that the variation remains within 0.1 % for 1000 consecutive iterations. More details

related to the experimental and computational methodology is provided in reference [11].

Validation

Experiments were conducted in a cascade wind tunnel to obtain the internal surface temperature data at different regions of the vane internal surface. The typical nozzle guide vane used in the present computational study is fabricated using high-quality acrylic material and used as the central vane in the cascade. Liquid crystal thermography technique is used to obtain the internal surface temperature. The color change is recorded by using a high definition camcorder and later processed in MATLAB to obtain the surface temperature. In order to validate the mesh and model exactly same boundary conditions are maintained for both experiment and computation. A detailed uncertainty analysis is carried out to consider the conduction losses in the coolant pipe and it is observed that the temperature difference across the coolant pipe is as less as 0.2 K. Keeping these small variations in mind all the temperature data are presented in non-dimensional form so that the temperature profile remains independent of the coolant and mainstream temperature. The uncertainty in the local temperature measurement will not be affected drastically, as the data acquired through thermocouple and TLC, is same. A good correspondence is seen between the average non-dimensional temperature $[\theta = (T_i - T_c)/(T_m - T_c)]$ distribution along the different region of the surface under study. A Maximum error of 8 % is observed between the experimental and computational data, as shown in Figure 4. More details related to the experimental procedure and results of validation are presented in reference [11].

Results and discussion

The minimum coolant flow rate at which the mainstream ingestion (at a Reynolds number of 7.2×10^5) can be prevented is found to be 0.0015 kg/s through AIT, with a corresponding Reynolds number of $Re_{AIT} = 44,737$; and 0.006 kg/s through FIT, i. e. $Re_{FIT} = 17,894$. The coolant flow rate is further increased to 1.2 and 1.5 times, to investigate the effect of coolant flow rate on vane internal surface temperature distribution and Nusselt number (hl/k) distributions. Similarly the effect of
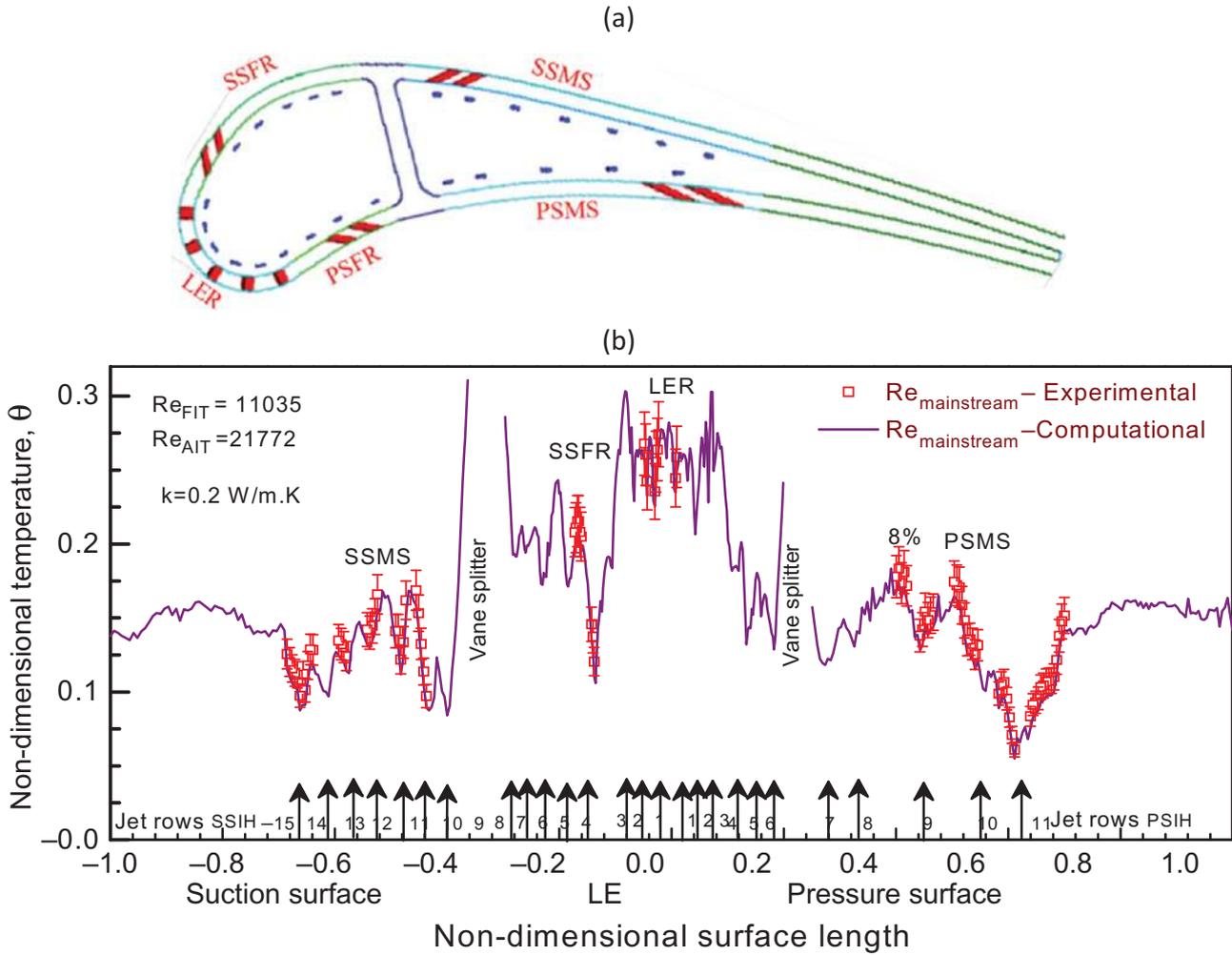
Figure 4: (a) Different regions of the vane surface (b) Experimental validation of present computational model at mainstream Reynolds number of 1.44×10^5.

mainstream Reynolds number is studied, at constant AIT and FIT coolant Reynolds numbers of 74,561 and 26,842 respectively. The mainstream Reynold number ($\rho.Vm.C/\mu$) is calculated by considering the vane chord length as characteristic length whereas the coolant Reynolds number ($\rho.Vc.D/\mu$) is calculated based on the coolant pipe diameter.

The effect of mainstream to coolant temperature difference ranging from 50.8 to 64.4 K, on the dimensional and non-dimensional temperature profile is also investigated. Note that the values of (Tc/Tm) ratio are maintained here according to Han et al. [12]. All the above investigations are carried out to determine the internal surface temperature distribution, with conjugate thermal conditions for three vane materials having conductivity values of 0.048, 0.2 and 1.1 W/m.K. The details of these variations are presented in Table 2. The temperatures in all figures are spanwise averaged values.

Table 2: Details of the parametric variations.

(i) Effect of coolant flow rate ($T_m = 339$ K, $T_c = 288$ K, Re mainstream $= 4.8 \times 10^5$)

Material conductivity (W/m.K)	Flow rate in AIT	Re_{AIT}	Flow rate in FIT	Coolant Re_{FIT}
1.1	0.015	44,737	0.006	17,894
	0.018	53,684	0.0072	21,473
	0.025	74,561	0.009	26,842

(ii) Effect of mainstream Reynolds number ($T_m = 339$ K, $T_c = 288$ K, Re coolant AIT $= 74,561$, Re coolant FIT $= 26,842$)

Material conductivity (W/m.K)	Mainstream Reynolds number
1.1	4.8×10^5
	6.04×10^5
	7.2×10^5

(iii) Effect of temperature difference for the chosen materials
($Re_{mainstream} = 4.8 \times 10^5$, $Re_{coolant\ AIT} = 74,561$, $Re_{coolant\ FIT} = 26,842$)

Material conductivity (W/m.K)	Coolant Temperature (K)	Mainstream Temperature (K)	Temperature difference (K)
1.1	254	304.8	50.8
	288	345.6	57.6
	322	386.4	64.4

(iv) Effect of conductivity ($T_m = 339$ K, $T_c = 288$ K)

Material conductivity (W/m.K)	Mass flow in AIT Chamber	Coolant Re_{AIT}	Mass flow in FIT Chamber	Coolant Re_{FIT}	$Re_{mainstream}$
0.048	0.015	44,737	0.006	17,894	4.8×10^5
	0.025	74,561	0.009	26,842	7.2×10^5
0.2	0.015	44,737	0.006	17,894	4.8×10^5
1.1	0.015	44,737	0.006	17,894	4.8×10^5
	0.025	74,561	0.009	26,842	7.2×10^5

shown in Figure 5. In general, the internal surface temperature distribution shows maximum temperature at the leading edge and it starts decreasing towards the trailing edge region. Continuous peaks and valleys are observed due to jet impingement effect. The temperature value shows a drop because of higher impingement velocity, along a particular jet row. Between any two impinging jet rows, the peak temperature is observed where the coolant velocity is minimum. Due to the presence of vane splitter, which separates the FIT and AIT chambers, a gap exists in the plot. With the increase in the coolant Reynolds number, the internal surface temperature decreases. However, the decrease in surface temperature is not uniform in all the regions of the interior vane surface. In order to get a quantitative idea, the surface averaged temperature values along the different region of the vane internal surface, are presented in Table 3. It is found that the leading edge region shows the least percentage decrease in the internal surface temperature, whereas the pressure surface trailing edge region shows maximum decrease in surface temperature.

Effect of coolant flow Reynolds number on internal surface temperature

The effect of coolant mass flow rate on the spanwise averaged vane internal temperature variations are

Effect of coolant flow Reynolds number on internal surface Nusselt numbers

The effect of coolant flow Reynolds number on spanwise averaged Nusselt number is shown in Figure 6. In general,
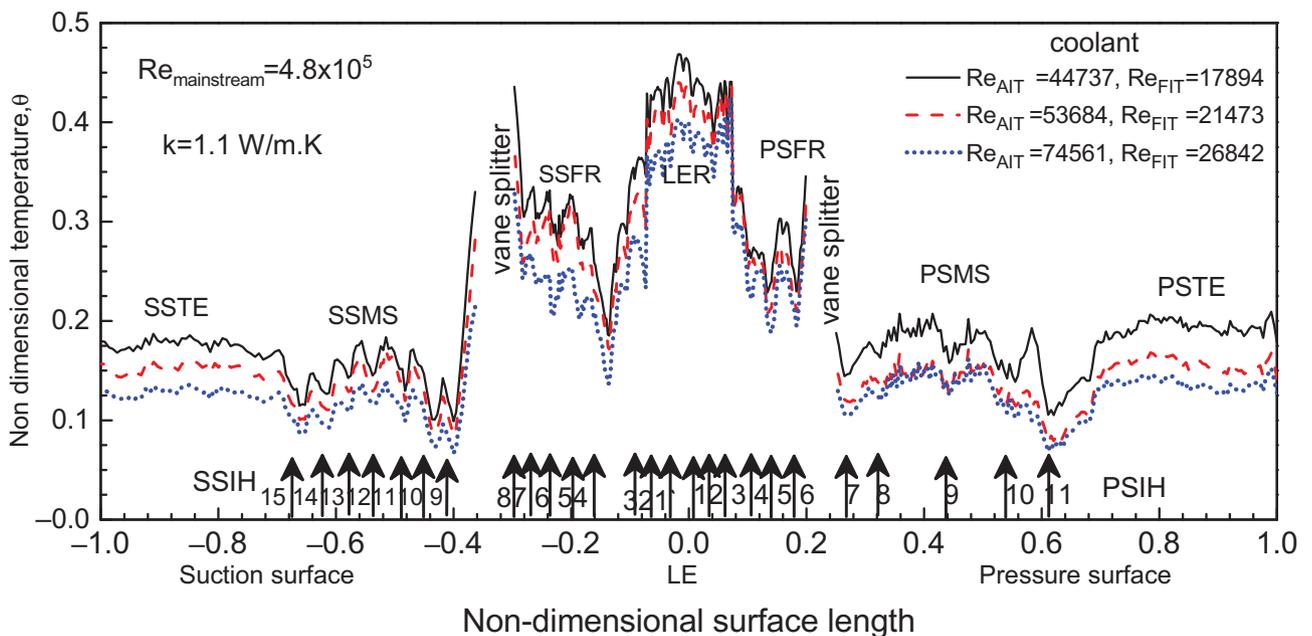

Figure 5: Effect of coolant flow rate on non-dimensional surface temperature distribution.

Table 3: Effect of coolant flow Reynolds number, on surface average temperature along different regions of the NGV.

| Regions	NDL		$k = 1.1$ W/m.K			Percentage variation
			Non-dimensional temperature		$Re_{AIT} = 44{,}737$ to $53{,}684$ $Re_{FIT} = 17{,}894$ to $21{,}473$	$Re_{AIT} = 44{,}737$ to $74{,}561$ $Re_{FIT} = 17{,}894$ to $26{,}842$
		$Re_{AIT} = 44{,}737$ $Re_{FIT} = 17{,}894$	$Re_{AIT} = 53{,}684$ $Re_{FIT} = 21{,}473$	$Re_{AIT} = 74{,}561$ $Re_{FIT} = 26{,}842$		
PSTE	0.75 to 1	0.194	0.156	0.137	19.24	29.37
PS MS	0.37 to 0.75	0.166	0.131	0.122	21.11	26.60
PSFR	0.12 to 0.37	0.280	0.262	0.243	6.58	13.28
LE	−0.12 to 0.12	0.433	0.411	0.379	4.97	12.40
SSFR	−0.12 to −0.49	0.302	0.275	0.233	8.89	22.92
SS MS	−0.54 to −0.81	0.153	0.136	0.112	11.58	26.75
SSTE	−0.81 to −1	0.175	0.151	0.127	13.39	27.24
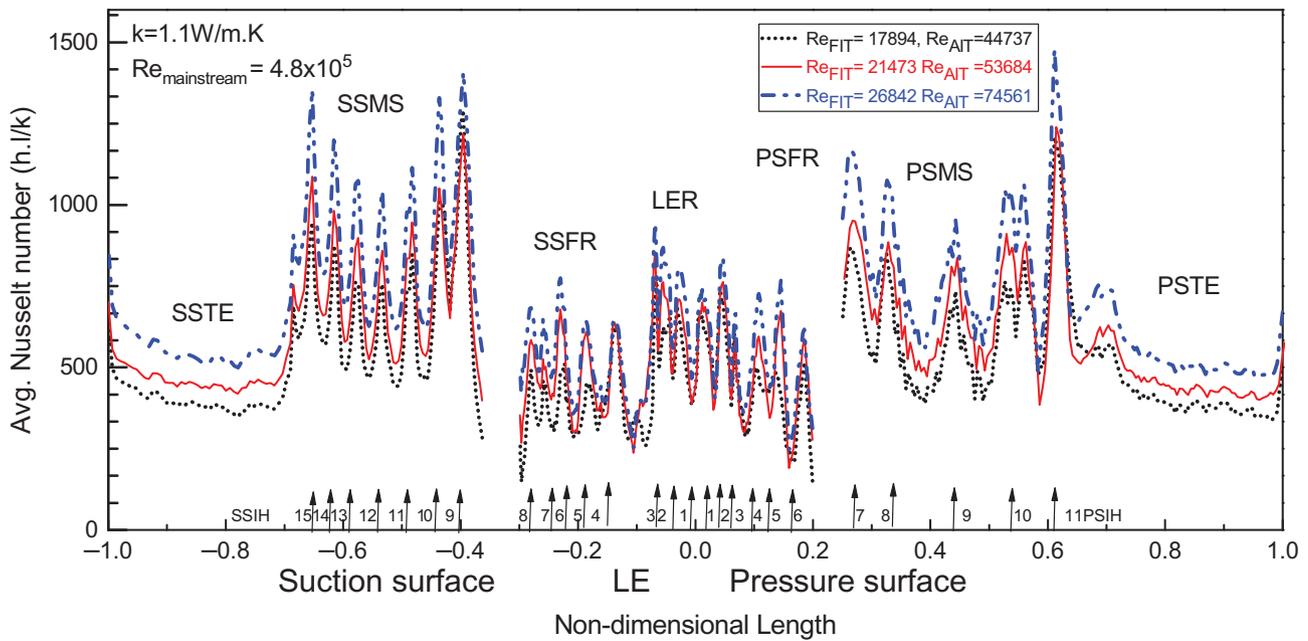
Figure 6: Effect of coolant flow rate on spanwise averaged Nusselt number distributions.

Nusselt number peaks are noticed at the jet impingement regions. Between two jet rows in the wall jet region, a large drop in Nusselt number is observed as the coolant velocity is low. Nusselt number shows lower values at the leading edge region (LER) and fillet region of the suction and pressure surfaces (SSFR and PSFR) than at the mid-span section. It is because the flow rate through the FIT chamber is lower than that through the AIT chamber. The FIT chamber coolant flow is kept low to prevent jet lift off near the leading edge region. In the trailing edge region, the Nusselt number distribution shows lower value compared to other regions. The Nusselt number distribution remains uniform in the trailing edge region as it is convection cooled and has no impinging jets. As the coolant flow rate is increased (1.2 times and 1.5 times) from the minimum flow rate, the spanwise averaged Nusselt number increases along each jet row. The midspan region of the suction surface shows seven peaks in Nusselt number distribution along the seven jet rows (SSIH 8 to 15) facing the suction surface. Similarly, the pressure surface shows five such peaks in Nusselt number. The average Nusselt number along the midspan region pressure surface shows higher peak value along jet row PSIH11 and on the suction surface midspan region along the jet row SSIH7. This is because of (i) higher impinging velocity along these impingement holes, which in turn is due to provision of convergent section of the AIT chamber, and (ii) presence of the row of film holes near the impinging jet.

Effect of coolant Reynolds number on vane temperature

The conduction within the solid NGV varies differently from leading edge to trailing edge. To understand this effect, the mainstream and coolant temperature distributions (Figure 7) are presented in the plane cut along the chord at the centre of the NGV. In the chosen plane, the film hole SH, SS4, SS6, PS2, and PS6 are noticeable. When the coolant Reynolds number is increased, the film coolant comes out of the film holes with higher velocity from the film hole SH. The coolant, after effusing out from the film hole, tend to move towards the suction surface because of the influence of adjacent film coolant coming from other film holes along the same row. The film hole row (SH) at stagnation zone is spanwise inclined from zero to 55° that forces the coolant to effuse out with different flow angle and velocity. When the coolant flow Reynolds number is increased from 21,473 to 26,842 in the FIT chamber, jet lift-off is caused at the film hole PS2. It creates an adverse effect on the external and internal surface temperature distributions. As seen in the pressure surface fillet region (PSFR), with the increase in FIT flow rate, the surface is exposed more to hot mainstream flow. As the coolant distribution over the vane external surface is uneven, the temperature within the vane solid changes in different regions. This is evident from Figure 8. Among different regions of the vane internal surfaces, the mainstream heat

conduction is more prominent in the leading edge region compared to all other regions. A sharp change in trailing edge region temperature is observed with increase in coolant flow rate. Between the pressure surface and suction surface, the pressure surface is more influenced by the mainstream. At maximum coolant flow Reynolds number, the internal side of NGV shows lower temperature throughout the NGV. It is indicated by blue patches.

Effect of mainstream Reynolds number on internal surface temperature

The internal surface temperature distribution shows sensitivity to mainstream Reynolds number variation, as indicated in Figure 9. The variation of average surface temperature along different regions of the NGV, with changing mainstream Reynolds number, is presented in Table 4. The internal side of leading edge region shows maximum temperature, which indicates maximum mainstream heat conduction and decrease in film coolant effectiveness on the external surface. However, the percentage increase in average surface temperature indicates a less increase in surface temperature at the leading edge when the mainstream Reynolds number is changed. The pressure surface midspan region shows an increase of 39 % in the averaged surface temperature, when mainstream Reynolds number is changed from $Re = 4.8 \times 10^5$ to
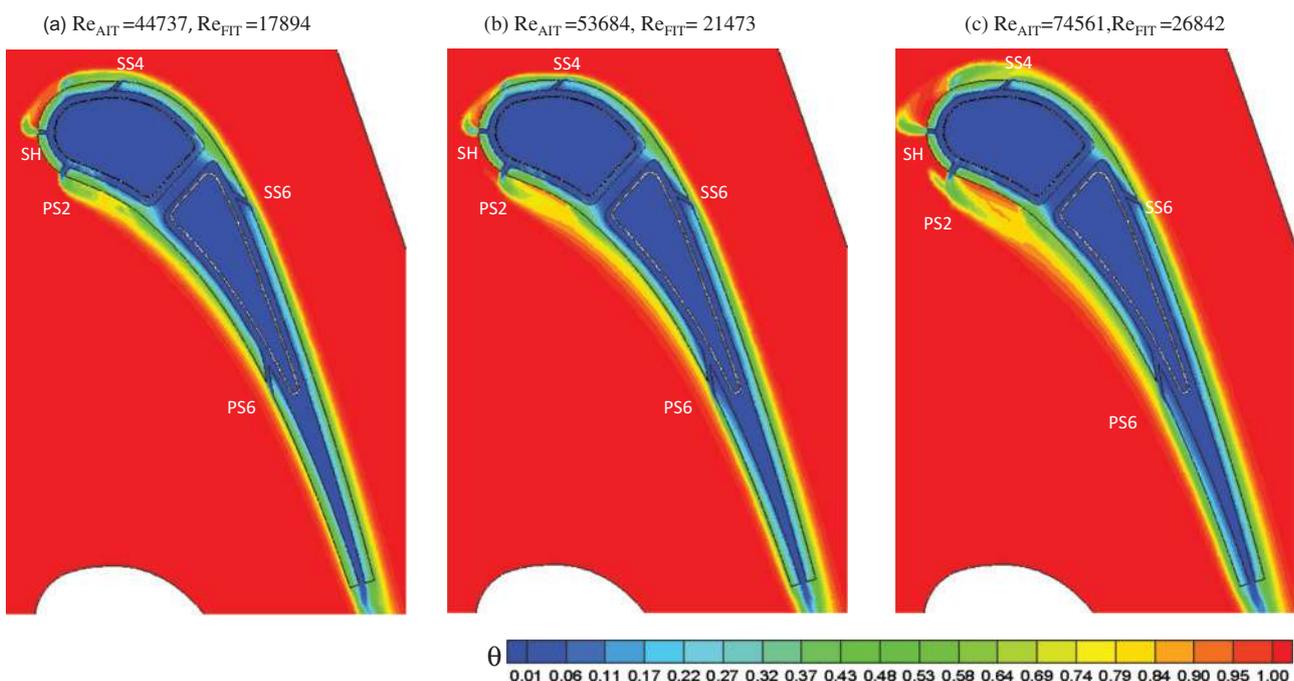

(a) $Re_{AIT} = 44737$, $Re_{FIT} = 17894$ (b) $Re_{AIT} = 53684$, $Re_{FIT} = 21473$ (c) $Re_{AIT} = 74561$, $Re_{FIT} = 26842$

θ 0.01 0.06 0.11 0.17 0.22 0.27 0.32 0.37 0.43 0.48 0.53 0.58 0.64 0.69 0.74 0.79 0.84 0.90 0.95 1.00

Figure 7: Temperature contours showing the effect of coolant Reynolds number on film coolant distributions at the center plane.
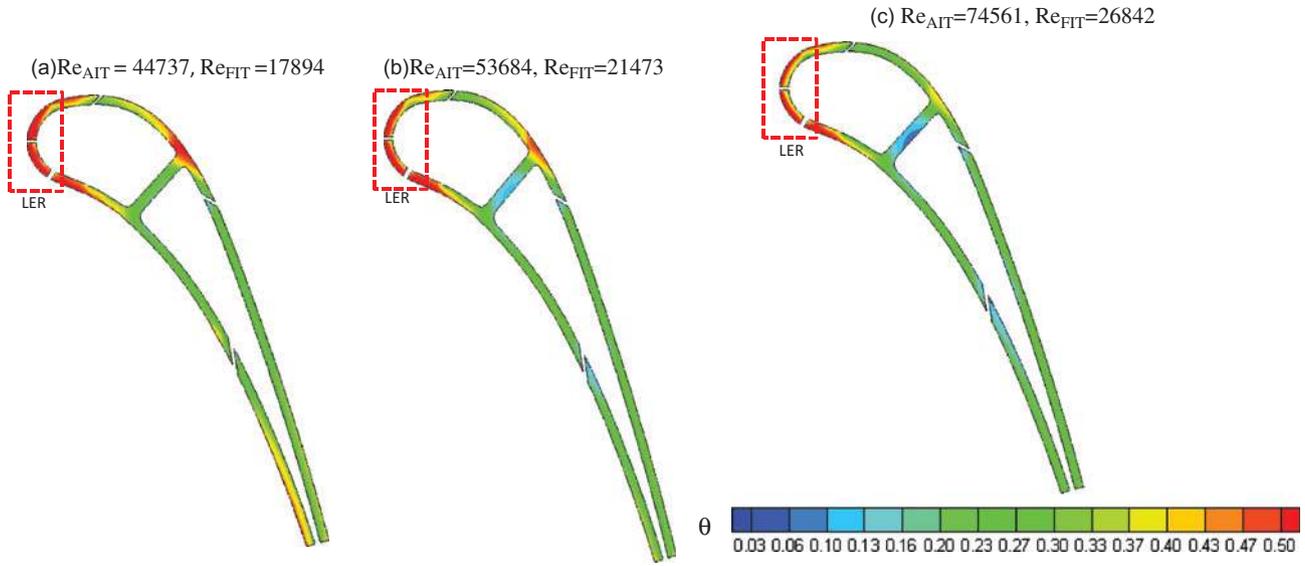
Figure 8: Effect of coolant Reynolds number within vane solid thickness for k = 1.1 W/m.K.
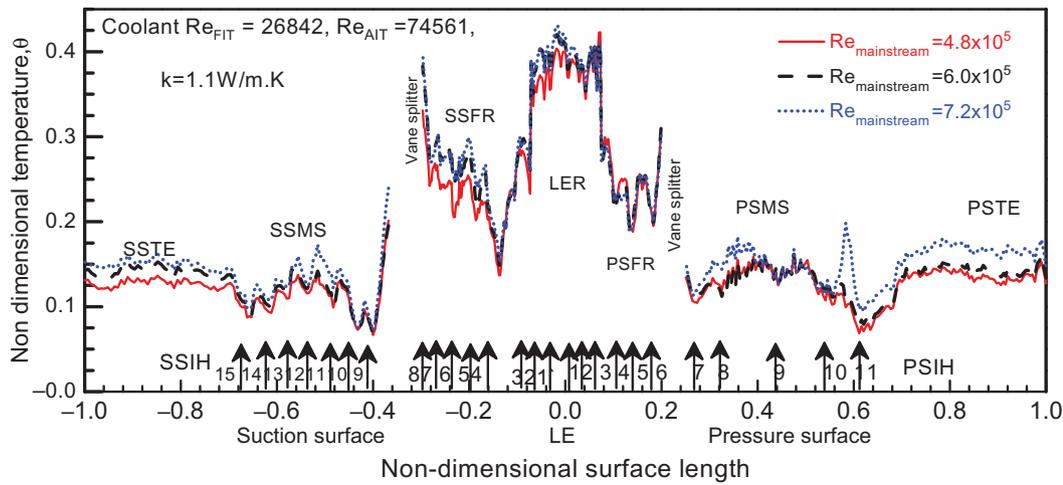

Figure 9: Effect of mainstream Reynolds number on non-dimensional temperature.

Table 4: Effect of mainstream Reynolds number on average non-dimensional temperature.

Regions	NDL		k = 1.1 W/m.K		Percentage variation in non-dimensional temperature	
		Non-dimensional temperature				
		$Re = 4.8 \times 10^5$	$Re = 6.04 \times 10^5$	$Re = 7.2 \times 10^5$	$Re = 4.8 \times 10^5$ to 6.04×10^5	$Re = 4.8 \times 10^5$ to 7.2×10^5
PSTE	0.75 to 1	0.137	0.144	0.171	5.06	24.88
PS MS	0.37 to 0.75	0.122	0.131	0.169	7.70	39.26
PSFR	0.12 to 0.37	0.243	0.251	0.260	3.27	6.74
LE	−0.12 to 0.12	0.379	0.392	0.396	3.45	4.50
SSFR	−0.12 to −0.49	0.233	0.255	0.260	9.26	11.43
SS MS	−0.54 to −0.81	0.112	0.117	0.129	4.40	15.06
SSTE	−0.81 to −1	0.127	0.141	0.150	11.08	17.80

$Re = 7.2 \times 10^5$. Similar variations are also observed near the suction surface fillet region, at $Re = 6.04 \times 10^5$ and $Re = 7.2 \times 10^5$. The trailing edge region shows highest percentage increase, in internal surface temperature.

Effect of mainstream Reynolds number on vane temperature

The heat conduction within the solid is affected by the mainstream Reynolds number because the film coolant distribution varies from the leading edge to trailing edge. To analyse these effects, a plane is cut in the chord-wise direction at the centre of the NGV of the vane. In this plane, the effect of increasing mainstream Reynolds number on film coolant distribution is presented as shown in Figure 10. The film coolant distribution in the chosen plane indicates that for all three mainstream Reynolds number the suction surface is better cooled compared to the pressure side. The lower pressure on the suction side of the vane leads to a higher thickness of film coolant distribution which helps in increasing the external effectiveness and decreasing the internal temperature. However, on the pressure side, reduced thickness of the film is observed for the minimum Reynolds number ($Re = 4.8 \times 10^5$) case. As Reynolds number increases the film thickness decreases on both the pressure and suction sides of the vane. The film coolant from the leading edge

centre hole (SH), after effusing out, tends to move towards the suction side. This results in exposing the lower half of the leading edge (pressure side) directly to the mainstream. This behaviour is noticed for all three main-stream Reynolds numbers. The jet lift-off from the film hole PS2 is suppressed at the mainstream Reynolds number, $Re = 7.2 \times 10^5$. Further, it gives better film coolant distribution near the pressure surface fillet region, which in turn reduces the internal surface temperature.

In Figure 11, the variation of heat conduction within the solid for the three mainstream Reynolds number is presented. It is observed that the heat conduction phenomenon varies from leading edge region to trailing edge region, due to uneven coolant distribution at different Reynolds number. The leading edge region (LER) is directly exposed to mainstream, due to the jet lift-off phenomena. Therefore, higher temperature is expected in this region. However, at higher Reynolds number the external effectiveness increases due to reduction in the effect of jet lift-off. Similarly, near the suction surface fillet region (SSFR) lower internal surface temperature is observed, when the mainstream Reynolds number increased to $Re = 6.04 \times 10^5$. This is due to a reduction in jet lift-off from the film hole SS4, which causes better film coolant distribution. When the mainstream Reynolds number is further increased to 7.2×10^5, the midspan region of pressure and suction surfaces shows better uniformity in temperature distribution.
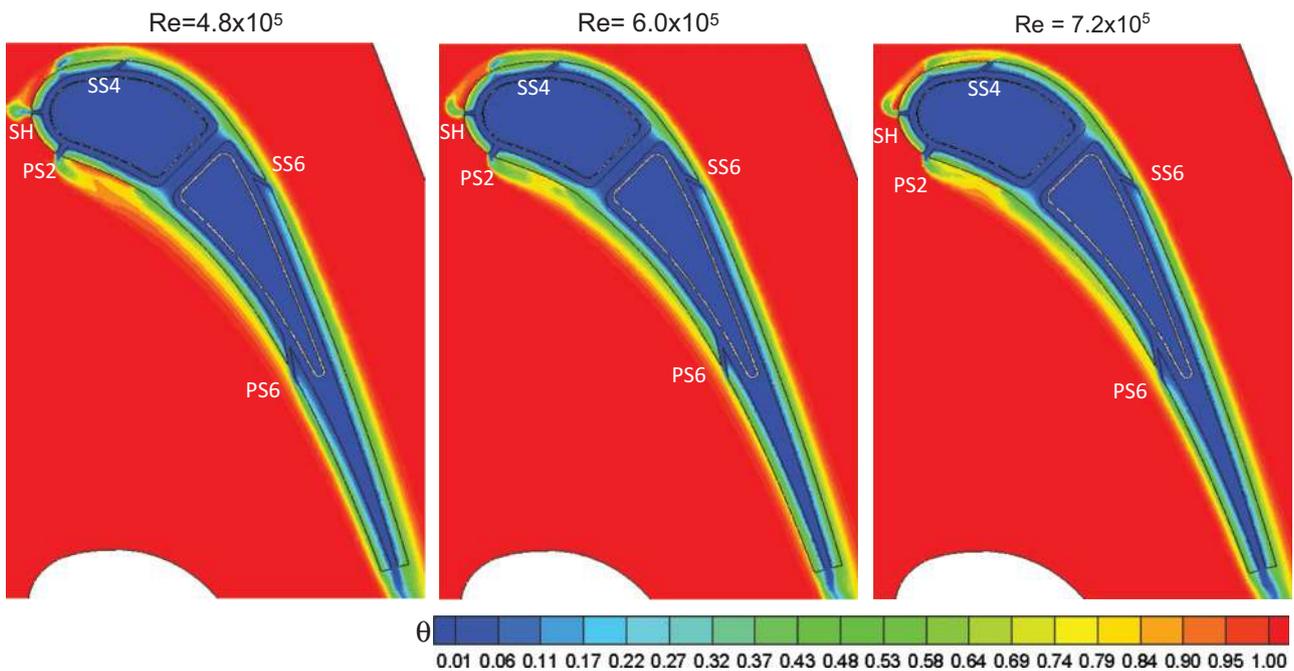

Figure 10: Temperature contours showing the effect of mainstream Reynolds number on film coolant distributions at the centre plane.
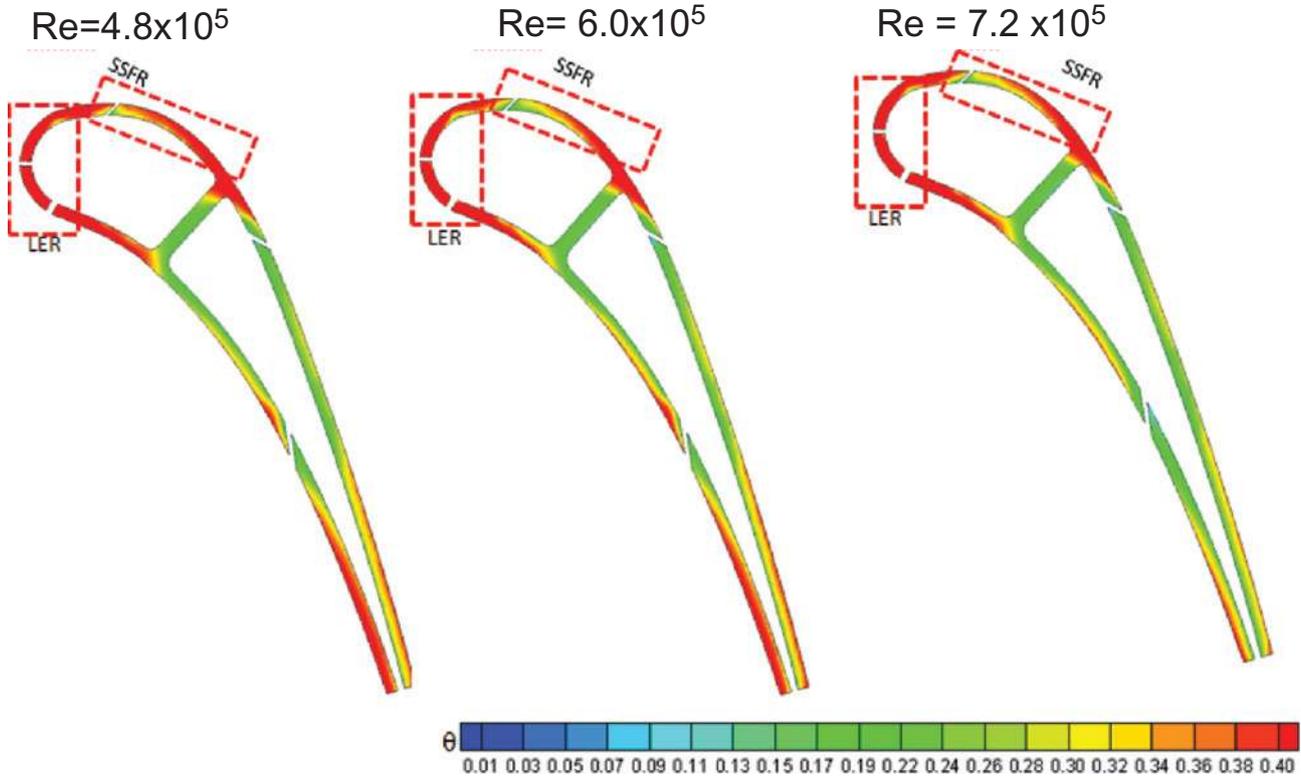
Figure 11: Effect of mainstream Reynolds number within vane solid thickness for k = 1.1 W/m.K.

Effect of mainstream to coolant temperature difference

The mainstream and coolant temperatures are changed systematically with temperature differences of 50.8 K, 57.6 K, and 64.4 K, to understand the behaviour of temperature distributions. The dimensional internal surface temperature distribution is presented in Figure 12. Considerable difference in dimensional internal surface temperature is observed as the coolant and mainstream
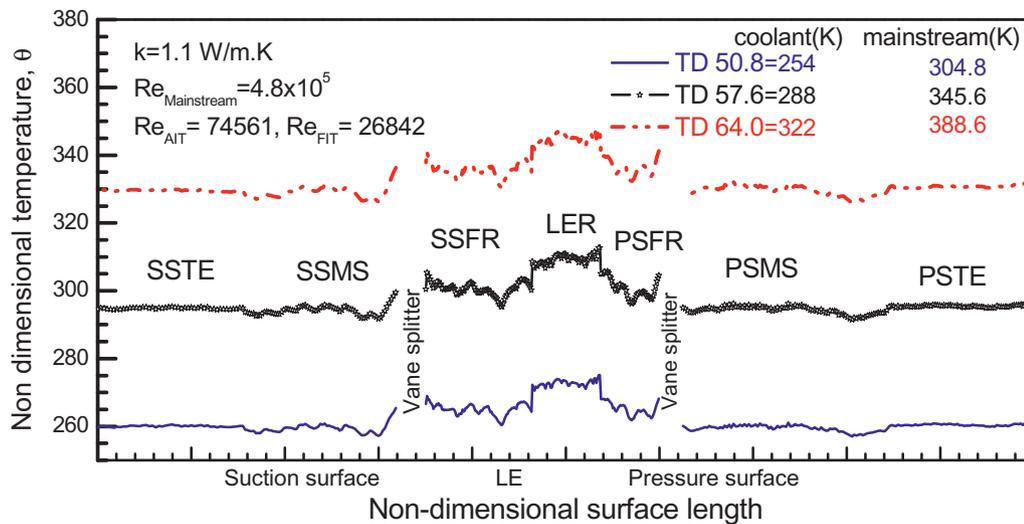

Figure 12: Dimensional temperature profile with changing mainstream and coolant temperature.
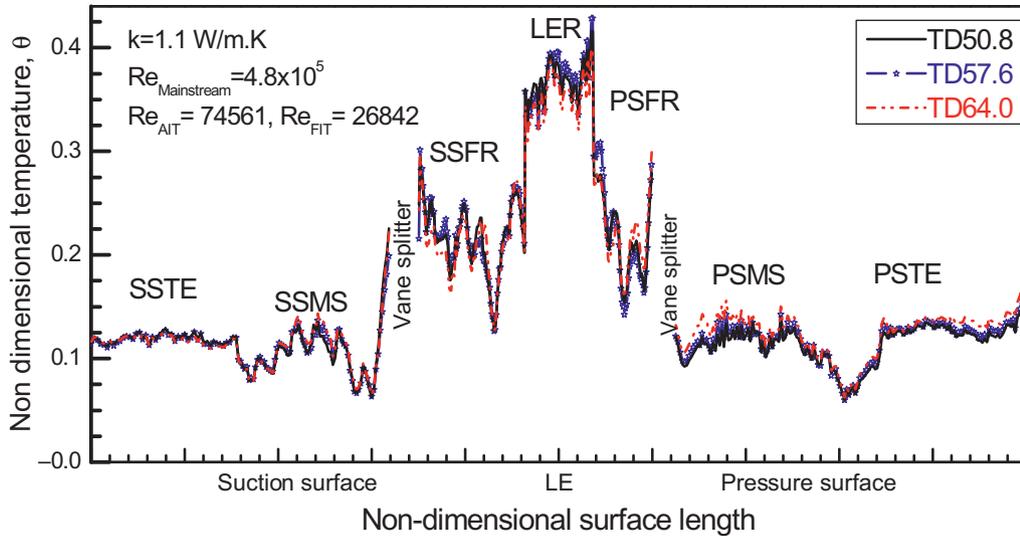
Figure 13: Non- dimensional temperature profile with changing mainstream and coolant temperature.

are maintained at different temperatures. The non-dimensional surface temperature profiles for the three materials are presented in Figure 13. It is noticed that, though the temperature difference is changed, the non-dimensional temperature lines fall on each other. It indicates that the variation in the mainstream to coolant temperature does not affect the non-dimensional temperature distribution. As the non-dimensional temperature profiles remain independent of the coolant and mainstream temperature changes, it is concluded that the results of the scaled up model apply to the prototype as well.

Effect of vane conductivity on internal surface temperature

Figure 14 shows the internal surface temperature distributions for the three materials where both mainstream (4.8×10^5) and coolant Reynolds number ($Re_{AIT} = 44,737$ and $Re_{FIT} = 17,894$) are kept constant. The higher conductivity material shows higher internal surface temperature. Considering that for given material conductivity the ratio between maximum temperatures to minimum temperature indicates the temperature gradient which exists on the surface, the gradient is higher for the
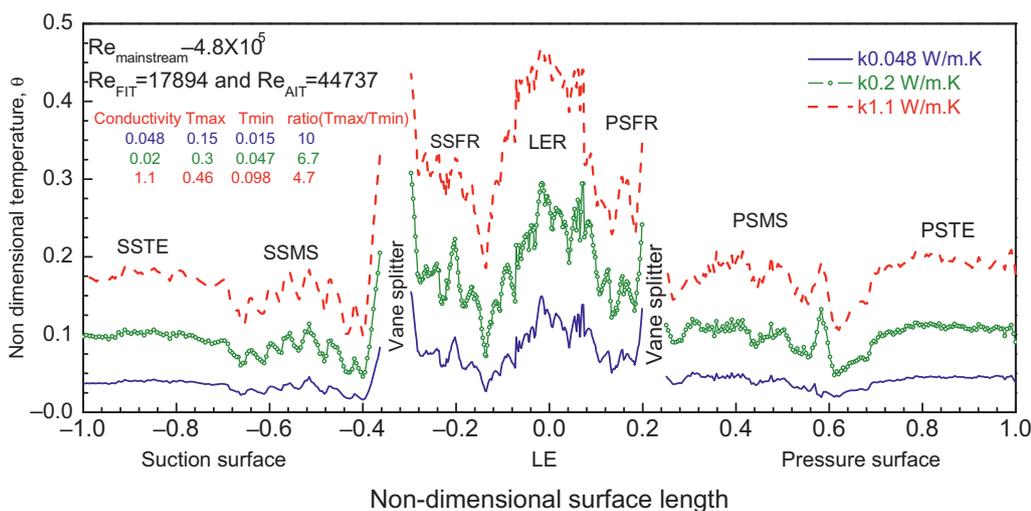

Figure 14: Effect of conductivity on non-dimensional surface temperature distribution.
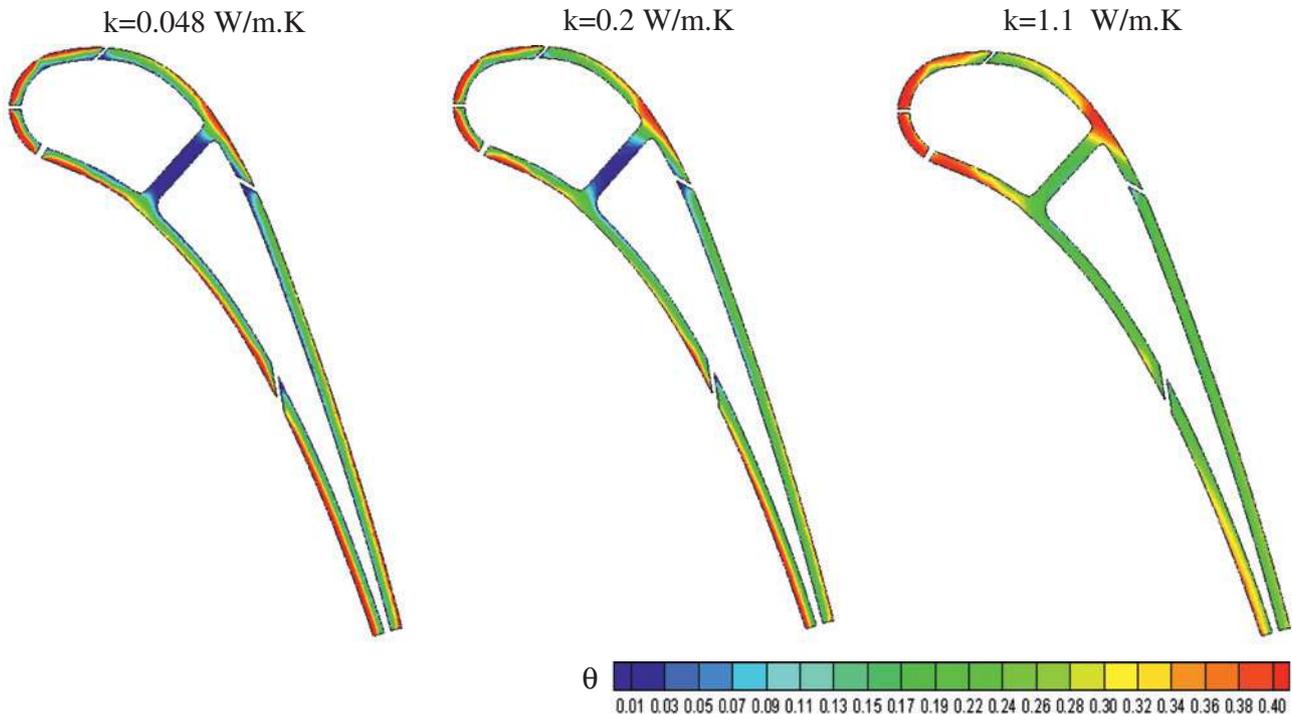
Figure 15: Effect of conductivity on temperature distributions within solid thickness of the vane.

lower conducting material and the gradient decreases as conductivity increases. This is evident from Figure 15 where the temperature gradient within the solid thickness of the vane is presented across the mid-section plane of the NGV. The temperature gradient across the solid is more for the lower conductivity material, as the external side shows very high temperature ($\theta = 0.5$ near leading edge region) and the internal side shows low temperature ($\theta = 0.03$). This large gradient in temperature across the vane surface temperature is undesirable as it leads to high thermal stress within the vane. In case of higher conductivity material, though the internal surface temperature is high, the solid temperature gradient are low, which makes it more suitable for its use as a vane material.

The effect of increase in coolant mass flow rate for the lower and higher conductivity materials are compared in Figure 16. As the coolant flow rate is increased 1.5 times ($Re_{AIT} = 74,561$, $Re_{FIT} = 26,842$) from minimum flow rate ($Re_{AIT} = 44,737$, $Re_{FIT} = 17,894$), the surface temperature decreases for both materials. However the percentage decrease in average surface temperature is more for the lower conducting material, as compared to the higher conducting material. This is due to lower heat flux values at the interior surface compared to the higher conductivity material. For the higher conductivity material the internal

surface heat flux values are high, as the mainstream heat conducts easily through the solid.

Figure 17 shows the effect of increase in mainstream Reynolds number for the lower and higher conductivity materials. As the mainstream Reynolds number is from 4.8×10^5 to 7.2×10^5 increased the higher conductivity material shows more sensitivity to internal surface temperatures compared to lower conductivity material. The leading edge region shows less variation in average surface temperatures for both the materials.

Effect of vane conductivity on internal surface Nusselt numbers

As the vane conductivity changes from k = 0.048 to k = 1.1 W/m.K, the internal Nusselt number distribution (Figure 18) shows less than 6 % variation. This trend clearly indicates the importance of carrying out conjugate heat transfer analysis for the NGV. In the case of conjugate heat transfer analysis, changing material conductivity leads to changes in the surface heat flux (q″) values and surface temperature, which results in the nearly constant values of heat transfer coefficient. However, the surface temperature values change
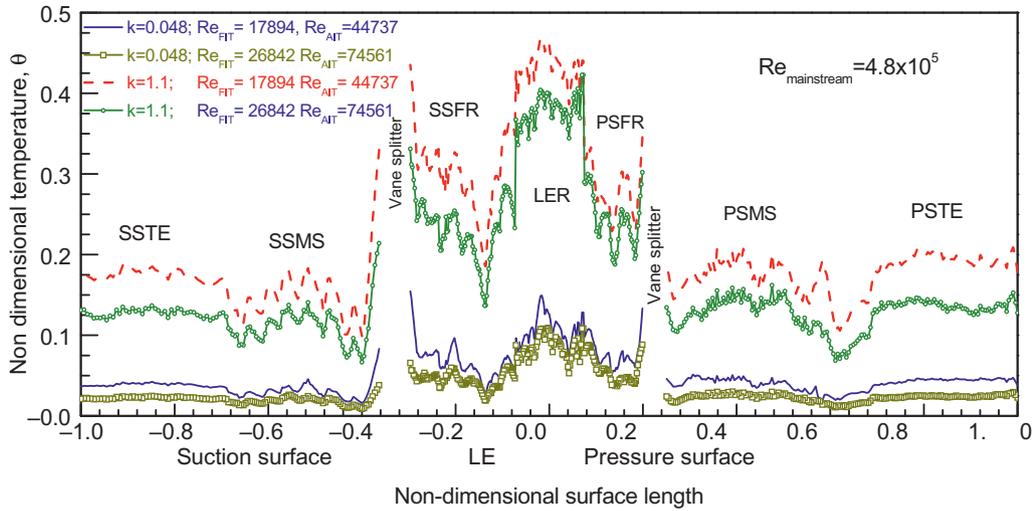
Figure 16: Effect of conductivity on surface temperature distribution with changing coolant Reynolds number.
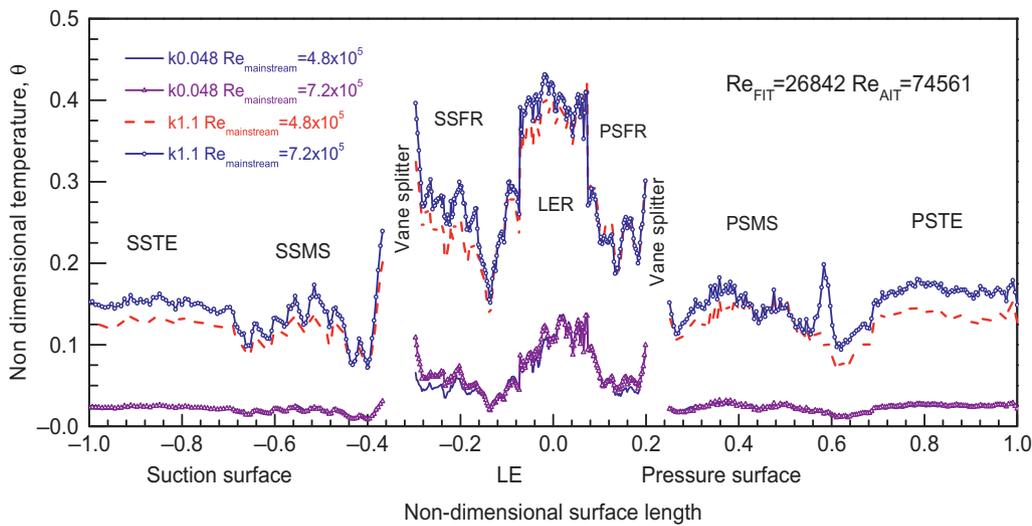

Figure 17: Effect of conductivity on internal surface temperature distribution with changing mainstream Reynolds number.
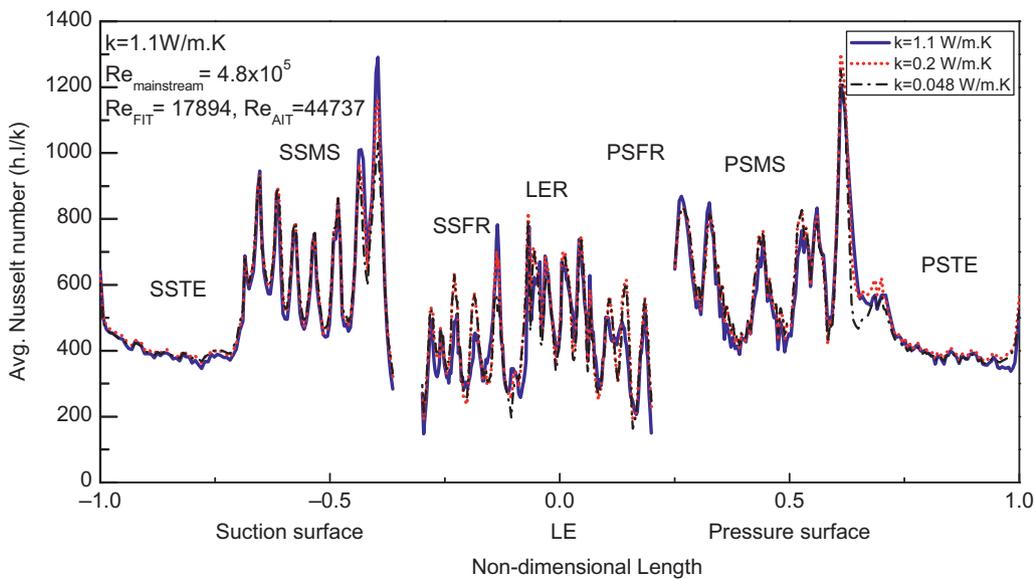

Figure 18: Effect of conductivity on internal Nusselt number distribution.

drastically with changing the material conductivity. In case of gas turbine nozzle guide vane, the focus is to find out the location of hot patches, as well as the temperature gradient, so that the region of thermal stress can be identified.

As the non-dimensional temperature, profiles remain independent of the coolant and mainstream temperature changes, the results of the scaled up model apply to the prototype as well.

Conclusions

Internal heat transfer studies under conjugate boundary condition are carried out on a typical nozzle guide vane with combined impingement and film cooling. The effect of conductivity variation is studied by systematically varying both coolant and mainstream Reynolds number on the NGV internal surface temperature distribution. The values of material thermal conductivity are chosen to satisfy the matched Biot number criterion, so that the non-dimensional temperature profile is valid for engine conditions.

The major conclusions of the present investigation are listed in the following:

1. The local temperature distribution within the vane solid largely depends on the coolant flow distribution on the internal and external side of the vane.
2. For a given mainstream Reynolds number and coolant flow rate, the temperature gradient is higher for the lower conductivity material, and the gradient decreases as conductivity increases. Therefore, it is desirable to use higher conductivity materials among the suitable ones, for vane design.
3. The internal surface temperature of the lower conductivity material shows the least increase in internal surface temperature with increase in mainstream Reynolds number; whereas the higher conductivity material shows more sensitivity to the variation in mainstream Reynolds number. As the conductivity increases, temperature of the vane internal surface is affected more significantly by the variation in the mainstream Reynolds number.
4. The spanwise averaged Nusselt number distribution along the internal surface shows about 6 % variations with changing material conductivity. However, the surface temperature distributions of the materials show considerable variations. This point to the importance of carrying out conjugate analysis to predict the actual location of hot patches.
5. When the mainstream to coolant temperature difference (temperature gradient across the vane) changes the non-dimensional temperature profile remains same, but the dimensional temperature profile shows large variation in internal surface temperature.

Nomenclature

Bi	Biot number, non-dimensional
C	Vane hord, m
d	Jet diameter, m
D	Coolant pipe diameter, m
h	Heat transfer coefficient, W/m^{2}K
h_i	Heat transfer coefficient of internal surface, W/m^{2}K
h_e	Heat transfer coefficient of external surface, W/m^{2}K]
H	Distance between jet hole and target surface, m
k	Thermal conductivity, W/m.K
l	Span length, m
m	Mass flow, kg/s
Nu	Nusselt number, non-dimensional
q″	Heat flux
Re	Reynolds number, non-dimensional
S	Distance along the vane surface from leading edge, m
$S_{p.max}$	Distance along pressure surface from leading edge to trailing edge, m
$S_{s.max}$	Distance along suction surface from leading edge to trailing edge, m
T	Temperature, K
t	Thickness of vane, m
V	Velocity

Greek symbols

ρ	Density, kg/m^3
κ	Turbulent kinetic energy, m^2/s^2
ω	Specific dissipation rate, 1/sec
μ	Coefficient of viscosity, N s/m^2
φ	Overall effectiveness, $(T_m\text{-}T_e)/(T_m\text{-}T_c)$
θ	Non-dimensional temperature, $(T_i\text{-}T_c)/(T_m\text{-}T_c)$

Subscripts

amb	Ambient
c	Coolant
e	External
f	Fluid
i	Internal
m	Mainstream
s	Solid
w	Wall

Abbreviations

AIT	Aft Impingement Tube
DH	Hydraulic Diameter
FIT	Front Impingement Tube
HTC	Heat Transfer Coefficient
LER	Leading Edge Region
NDL	Non-Dimensional Length, (= S/S$_{s.max}$, S/S$_{pmax}$)
NDT	Non-Dimensional Temperature, θ

NGV	Nozzle Guide Vane
PSIH	Pressure Surface Impingement Hole
PSMS	Pressure Surface Mid-Span
RANS	Reynolds Averaged Navier Stokes
SSFR	Suction Surface Fillet Region
SSIH	Suction Surface Impingement Hole
SSMS	Suction Surface Mid-Span
SST	Shear Stress Transport

References

1. Albert JE, Bogard DG, Cunha F, Adiabatic and overall effectiveness for a film cooled blade, *ASME Turbo Expo 2004*, pp. 251–259, 2004.
2. Mouzon BD, Terrell EJ, Albert JE, Bogard DG, Net heat flux reduction and overall effectiveness for a turbine blade leading edge, *ASME Turbo Expo 2005*, pp. 825–832, 2005.
3. Dees JE, Bogard DG, Ledezma GA, Laskowski GM, Tolpadi AK. Experimental measurements and computational predictions for an internally cooled simulated turbine vane. J Turbomachinery. 2012;134(6):061003.
4. Albert JE, Bogard DG. Measurements of Adiabatic Film and Overall Cooling Effectiveness on a Turbine Vane Pressure Side With a Trench. J Turbomachinery. 2013;135(5):051007.
5. Ravelli S, Dobrowolski L, Bogard DG, Evaluating the Effects of Internal Impingement Cooling on a Film Cooled Turbine Blade Leading Edge, *ASME Turbo Expo 2010*, pp. 1655–1665, 2010.
6. Nathan ML, Dyson TE, Bogard DG, Bradshaw SD. Adiabatic and overall effectiveness for the showerhead film cooling of a turbine vane. J Turbomachinery. 2013;136(3):031005–01 to 031005-09.
7. Montomoli F, Massini M, Yang H, Han JC. The benefit of high-conductivity materials in film cooled turbine nozzles. International Journal of Heat and Fluid Flow. 2012;34:107–116.
8. Panda RK, Prasad BVSSS. Conjugate heat transfer from an impingement and film-cooled flat plate. Journal of Thermophysics and Heat Transfer. 2014;28(4):647–666.
9. Williams RP, Dyson TE, Bogard DG, Bradshaw SD. Sensitivity of the Overall Effectiveness to Film Cooling and Internal Cooling on a Turbine Vane Suction Side. J Turbomachinery. 2013; 136(3):031006–01 to 031006-07.
10. Celik IB, Ghia U, Roache PJ, Freitas CJ, Coleman H, Raad PE. Procedure for estimation and reporting of uncertainty due to discretization in CFD applications. J Fluids Eng. 2008;130 (7):078001–01 to 078001-04.
11. Pujari AK, Internal Heat Transfer Studies in a Gas Turbine Nozzle Guide Vane with Combined Impingement and Film Cooling, Ph. D Thesis, Indian Institute of Technology, Madras, 2015.
12. Han JC, Dutta S, Ekkad S. Gas Turbine Heat Transfer and Cooling Technology, 1Ind edition ed. Boca Raton, London, New York: CRC Press, Taylor & Francis Group, 2012:1–30.